Heavy Ion Acceleration in ^{3}He-rich Solar Energetic Particle Events: New Insights from Solar Orbiter

G. M. Mason[1], I. Roth[2], N. V. Nitta[3], R. Bučík[4], D. Lario[5], G. C. Ho[1], R. C. Allen[1], A. Kouloumvakos[1], R. F. Wimmer-Schweingruber[6], and J. Rodriguez-Pacheco[7]

[1]Applied Physics Laboratory, Johns Hopkins University, Laurel, MD 20723 USA, glenn.mason@jhuapl.edu

[2]Space Sciences, University of California at Berkeley, Berkeley, CA 94720, USA

[3]Lockheed Martin Advanced Technology Center, Palo Alto, CA 94304 USA

[4]Southwest Research Institute, San Antonio, TX 78238, USA

[5]Heliophysics Science Division, NASA Goddard Space Flight Center, Greenbelt, MD 20771, USA

[6]Institut für Experimentelle und Angewandte Physik, Christian-Albrechts-Universität zu Kiel, Kiel, Germany

[7]Universidad de Alcalá, Space Research Group, Alcalá de Henares, Madrid, Spain

Submitted: *2023 June 28*

Running title: Heavy Ion Acceleration in ^{3}He-rich SEP events

Unified Astronomy Thesaurus concepts: Solar flares (1496) – Solar energetic particles (1491) -- Solar particle emission (1517) -- Solar abundances (1474) -- Solar magnetic fields (1503) – Solar magnetic reconnection (1504)

Abstract

We present Solar Orbiter energetic particle observations of two ^{3}He-rich events with features more clearly observed than in prior studies. The event of 2022 November 9 observed from 0.59 au contained hundreds of ultra-heavy ions (UH, mass >78 amu) whereas previous observations at 1 au have shown only an occasional count or two. The event of 2023 April 8 observed from 0.29 au fortuitously had very low ambient activity, making it possible to observe spectra from the ^{3}He acceleration mechanism without contamination, revealing extremely low H and ^{4}He intensities arriving simultaneously with other ions observed in typical ^{3}He-rich events. Taken together with previous studies we believe these data show that ^{3}He-rich events have a single acceleration mechanism that is responsible for the unique abundance features of ^{3}He, heavy ions, and UH ions. Considering the acceleration model of Roth and Temerin (1997) that heats the ions over a broad range of gyrofrequencies away from those damped by H and ^{4}He, we calculate reasonable fits to the observed abundances O-Fe. A key result is that high values of, e.g., Fe/O typical of such events is not due to preferential Fe heating, but on the contrary is due mainly to the depletion of O which at elevated temperatures has a charge-to-mass ratio in the region of the waves damped by ^{4}He. The model also naturally incorporates features of high ionization states and neutron-rich isotope enhancements that have been long-standing puzzles in observations of this type of flare.

1. Introduction

Solar Energetic Particle (SEP) events are intensively studied since they can produce high radiation levels in the inner solar system, and are of broader interest in the area of particle acceleration in astrophysical settings. Large (or gradual) SEP events are associated with flares on the Sun with subsequent coronal mass ejections (CMEs) driving interplanetary (IP) shocks that can accelerate particles to relativistic energies. Instruments in space revealed an additional class of smaller events associated with electron acceleration and type III radio bursts, as well as energetic ions whose composition was highly enriched in ^{3}He, and significantly enriched in heavy ions (e.g., reviews by Desai & Giacalone 2016; Reames 2018). The distinct compositional properties of ^{3}He-rich events have long been taken as indicators of an acceleration mechanism different from that in large SEP events and therefore of interest despite their small size. Generally speaking, shock acceleration is associated with large SEP events, while ^{3}He-rich events are associated with stochastic acceleration at sites where emerging magnetic flux reconnects with existing fields (e.g., reviews above and Petrosian 2012, 2008; Reames 2021). Advanced instruments with greatly improved mass resolution and much lower energy threshold revealed that ^{3}He-rich events are not rare as originally believed, but are extremely common with thousands each year during solar active periods (Wang et al. 2012; Wiedenbeck et al. 2005).

To further our understanding of how particles are accelerated at the Sun and released into interplanetary space, the Solar Orbiter mission probes closer to the Sun thereby enabling greatly improved observations of the sources (Müller et al. 2020). In the case of ^{3}He-rich events the closer distance not only increases the statistical accuracy of measurements, but also reduces uncertainties in source location and timing since the ions have shorter flight times to the spacecraft. In this paper we report improved observations of ^{3}He-rich events which, taken together with many prior observations at 1 au, allow us to address long-standing questions. For example, although heavy ion enrichments are clearly associated with these ^{3}He-rich events, the degree of ^{3}He enrichment and Fe enrichment are poorly correlated (e.g., Mason et al. 1986; Reames et al. 1994) thus raising the question whether the same mechanism accelerates both. A second example relates to the ionization states of the particles: the ^{3}He enrichment is widely believed to be due to its unique charge-to-mass ratio which might also favor partially ionized heavy ions. However, the measured heavy ion ionization states in ^{3}He-rich events are quite high, sometimes nearly fully stripped, and the enrichments grow with increasing charge state, the very opposite of expectations (e.g., review by Klecker et al. 2007). An additional open question regards the observation of ultra-heavy (UH, 78-228 amu) ions in surveys of ^{3}He-rich events (Mason et al. 2004; Reames 2000): are these extremely rare events (< 1 ion/day) actually associated with the ^{3}He-enrichment mechanism, and if so how can they be preferentially accelerated since their charge-to-mass ratio is much lower than Fe and lighter ions?

Below we report Solar Orbiter observations of two ^{3}He-rich events with greatly improved accuracy over prior work. These events exhibit the more common type of heavy ion enrichments as well as a smaller class of cases where the enrichments of Si and S are notably large. Following the model of Roth and Temerin (1997) for acceleration of ions over a broad range of charge-to-mass ratios by electromagnetic hydrogen cyclotron waves, we argue that many features of the heavy ion enrichments and ionization states can be reproduced by simple consideration of wave damping for fully stripped Q/M = 0.5 ions along with temperature increases as the plasma is heated in an acceleration event.

2. Observations

2.1 Instrumentation

The energetic particle observations reported here are from the Suprathermal Ion Spectrograph (SIS) which is part of the Solar Orbiter Energetic Particle Detector suite (Rodríguez-Pacheco et al. 2020; Wimmer-Schweingruber et al. 2021). SIS is a time-of-flight mass spectrometer that measures ion composition from H through ultra-heavy nuclei over the energy range ~0.1-10 MeV nucleon^{-1}. SIS has 2 identical telescopes, one facing sunward (telescope a) and the other anti-sunward (telescope b). In this paper the sunward telescope was used in order to reduce propagation effects. We also consulted data from the Solar Orbiter Radio and Plasma Wave investigation (RPW; Maksimovic et al. 2020), X-ray data from the Solar Orbiter Spectrometer/Telescope for Imaging X-rays (STIX; Krucker et al. 2020), EUV data from the Solar Orbiter Extreme Ultraviolet Imager (EUI; Rochus et al. 2020) and the Solar Dynamics Observatory (SDO) Atmospheric Imaging Assembly (AIA; Lemen et al. 2012). Solar Orbiter's magnetic connection to the Sun was estimated using the interplanetary magnetic field and solar wind data when available, and a Potential Field Source Surface (PFSS) model of the coronal field (Rouillard et al. 2020).

2.2 The 2022 November 9 and 2023 April 8 ^{3}He-rich SEP events

Table 1 shows properties of the two events discussed here. In both cases Solar Orbiter was magnetically connected to the Sun on the Earthward hemisphere, with separation angles from Earth to the west of the Earth-Sun line as shown. The Active Region (AR) associations are uncertain since the remote sensing data showed no clear signatures, but rather low levels of activity with some small jets located a few degrees from the ARs. Radio data showed some type III activity but no clean events as might be expected for two particle events that were very clearly observed. Particle detectors on ACE and STEREO had magnetic connection somewhat close to the events, but saw nothing for Event #1 (2022 November 9), and only a weak event at ACE for Event #2 (2023 April 8), roughly a factor of 10 below the Solar Orbiter instrument intensities as might be expected given the factor of ~3 larger radial distance of ACE. Lacking other signatures, ion injection times shown in the table were obtained from a "time shift analysis" in which ion data was shifted earlier according to particle speed using trial magnetic field lengths until ions over the whole energy range all lined up reasonably to a single injection time (e.g., Kollhoff et al. 2021). The deduced field line lengths were 0.57 and 0.38 au for events 1 and 2, respectively, while the nominal Archimedes spiral distances are 0.61 and 0.29 au for 400 km s^{-1} solar wind. The injection time uncertainties are estimated by assuming a 10% variation in field length.

Figure 1 shows SIS observations for 2022 November 9. The top panel shows intensities of H, ^{3}He, ^{4}He, O and Fe from the sunward facing telescope. Both H and ^{4}He were elevated due to prior activity, and their intensities rose only a factor of ~2. ^{3}He, Fe and O rose over two orders of magnitude over background, with Fe exceeding the ^{4}He intensity by a factor of ~2, a very unusual occurrence. The middle panel shows mass tracks with clear ^{3}He signature along with heavy ions. The bottom panel spectrogram shows 1/ion speed versus time, with clear velocity dispersion. The more intense portion of the 1/ion speed spectrogram extrapolates to the 06:28 UT injection time in Table 1, but it can be seen that there appears to be a smaller injection preceding this with approximate injection time of 05:31 UT. For masses above 50 amu, the ratio of events from the sunward to anti-sunward telescopes was >20:1.

The high Fe abundance in the 2022 November 9 event was accompanied by a large number of UH ions shown in Figure 2 (top panel), where filled red circles show the SIS mass histogram above

100 keV nucleon^{-1}. Above 100 amu where there are only single counts, the SIS data has been smoothed with a 20-bin running average. Although individual mass peaks are not resolved, the broad peaks in the SIS data for 78-100 and 125-150 amu are similar to features seen in solar system abundances (Anders & Grevesse 1989). The thin blue line in the panel is the mass histogram from the ACE survey (Mason et al. 2004), normalized to the Fe peak. The SIS and ACE histograms are similar but relative to Fe the SIS abundances are ~5 times higher than ACE. Although the ACE counting statistics are ~10 times higher than for SIS, they were summed over 295.7 days when Fe/O was elevated and UH enhancement could be expected (for details see Mason et al. 2004), whereas the SIS data were summed over roughly 12 hours. The bottom panel of Figure 2 repeats the 1/ion speed arrival distribution from Figure 1, overplotted with filled red circles for each ion of mass > 80 amu. The similarity of the arrival times is consistent with the UH nuclei being accelerated, released, and propagated simultaneously with the heavy ions 10-70 amu which make up the spectrogram, and therefore were likely accelerated in the same event. Such a correspondence between UH nuclei and heavy ions has not been seen before since prior observations at 1 au registered only single or very small numbers of counts for each accumulation period.

SIS observations for the event starting 2023 April 8 are shown in Figure 3. Solar Orbiter was close to perihelion and the prior background was extremely low. The intensity increases associated with the event were roughly two orders of magnitude. The striking similarity of the time-intensity profiles indicates that the species were all from a common event. Nevertheless, this is a very small event: the peak Fe intensity is roughly a factor of 100 lower than the 2022 November 9 event. The middle panel mass tracks show relatively high counts in the Si-S region. The middle panel energy threshold is 0.2 MeV nucleon^{-1}, lower than usual since setting the threshold higher leaves the panel largely empty of nuclei heavier than He. The bottom panel shows the 1/ion speed arrival distribution showing clear velocity dispersion. There is a hint of a somewhat earlier very weak injection as well. There are brief “dropouts” around 03:05 UT and 04:18 UT on April 9 where magnetic connection to the source is temporarily lost (e.g., Ho et al. 2022). Above 100 keV nucleon^{-1} and 50 amu, the ratio of the events from the sunward to anti-sunward telescopes was 10:1.

2.3 Mass histograms for the C-Fe region

Abundance enhancements in the Si-S region in the 2023 April 8 event are more easily seen in Figure 4 which shows mass histograms for both events for ion energies above 150 keV nucleon^{-1}. In order to facilitate the comparison, the y-axis scale has been adjusted so that the O peak is visually about the same height in both panels. While we emphasize the Si-S region in this paper, note also the different relative abundances for C and N in the two panels. The events with enhanced Si-S appear to be a distinct subset of all ^{3}He-rich events. The first reported event enhanced in Si-S as shown in the figure was on 1977 October 12-13 (see Fig. 9 in Mason et al. 1980), which was overlooked when a report of three such events found in 1997-2002 was published (Mason et al. 2002). More recently, a survey found 16 such events over the period 1999-2015, establishing their rare but continued appearance (Mason et al. 2016). Some ^{3}He-rich events observed on Solar Orbiter have also been rich in Si-S (e.g., event #5 in Bučík et al. 2023). Their small size is probably the reason they have not been reported from instruments with higher energy thresholds.

2.4 Differential energy spectra

Figure 5 shows **event averaged** differential energy spectra for the two events. The left panel shows the 2022 November 9 event which has a curved Fe spectrum of the type commonly seen in ^{3}He-rich events, but with the very unusual situation where the Fe spectrum exceeds ^{4}He. **The H and ^{4}He spectra were corrected by subtracting out the average ambient background before and after the event; this lowered the H intensity by a factor of ~3.5, and the ^{4}He intensity by a factor of ~2.5.** The He and heavier ion spectra do not extend beyond ~1 MeV nucleon^{-1}, with a slope of ^{4}He at the higher energies of -4.6. The right panel of Figure 5 shows the 2023 April 8 event, where the Fe and O spectra typically lie well below ^{4}He, but also where the ^{3}He spectrum exceeds the proton spectrum above 300 keV nucleon^{-1}. The higher energy ^{4}He spectral slope is -5.0. Because of the extremely low ambient intensities at the time of this event (Figure 3) these spectra are likely the best observations of energetic particles solely from a ^{3}He-rich SEP event, and show that the mechanism accelerates H and ^{4}He although apparently with low efficiency. The ULEIS instrument on ACE saw a few isolated counts from the 2023 April 8 event.

2.5 Comparison with prior surveys

Filled red circles in Figure 6 show the 160-226 keV nucleon^{-1} abundances for the 2 events, with protons from higher energy (due to threshold). The left panel for 2022 November 9 compares closely with the ^{3}He-rich event survey shown by the blue dashed blue line (Mason et al. 2004), except for H and ^{4}He which are >10 times lower. The Ca/O and Fe/O abundances are about a factor of 2 higher than the survey, but this is not unusual since elements further from the normalizing element tend to show larger dispersion. For example, the small blue dots at mass 56 show the individual event's Fe/O ratios in each survey, showing large variation. We conclude that for C-Fe the 2022 November 9 is a typical ^{3}He-rich event. The right panel of Figure 6 shows the abundance pattern in the 2023 April 8 event, where the observed abundances O and above (filled red circles) are reasonably close to the survey average of 16 high Si-S events (Mason et al. 2016). The high C and N abundances lie above the survey average, but such a pattern has been seen at least once previously (e.g., figure 2 in Mason et al. 2016). The small blue dots in the right panel at mass 56 show the individual events Fe/O ratios from the survey. Orange lines in the figure are from the model calculation discussed below.

3. Discussion

We consider these two events as representative of ^{3}He-rich events and discuss them as variations on a single mechanism, namely one that produces the "typical" pattern and a variation that shows high abundances of Si-S. In addition to the abundances, we will consider other features of ^{3}He-rich events, namely the ionization states measured at 1 au and the surprisingly large enhancements of neutron rich isotopes of Ne and Mg, which exceed by far those expected from the Fe/O ratios observed in ^{3}He-rich events (Dwyer et al. 2001).

Roth & Temerin (1997) and Temerin & Roth (1992) presented a model of ^{3}He and heavy ion enrichment in which particle acceleration is by electromagnetic hydrogen cyclotron waves in a single-stage process. Such waves have been observed in auroral plasmas associated with energetic electrons. Heavier ions can also be resonantly accelerated by the second or higher harmonics. The background magnetic field gradient is an important component of the process, wherein the magnitude of the acceleration is proportional to the field gradient. An important feature of the process is that due to the field gradient, particle cyclotron radii will change along the gradient allowing a single wave to accelerate a range of cyclotron frequencies. In effect this results in wide range of gyrofrequencies available for acceleration, rather than a specific narrow band described in most theories considered in review papers cited above. Like many other models considering

^{3}He-rich flares, this mechanism describes heating of a thermal population wherein the preferentially heated ions are subsequently injected into the energization process. **The presumed acceleration process could affect features such as maximum energy, spectral forms and energy dependences that are not addressed by the heating process discussed here**

3.1 Acceleration model

To preferentially heat heavy ions, Roth & Temerin (1997) assumed a wave power spectrum which covers the gyrofrequencies "between but not too close" to the H and ^{4}He frequencies, where presumably the wave amplitude is damped due to the high H and ^{4}He abundances. Figure 10 in their paper shows heavy ions of coronal elements available for acceleration in the range [0.28, 0.44] in units of H gyrofrequency, where the gyrofrequency of $^{4}He^{+2}$ is 0.5. In particular the figure showed increases in Si and S whose *Q/M* ratio falls in range of acceleration frequencies as temperatures increase above a few MK, which motivates the calculation here.

Figure 7 shows a plot of *Q/M* ratios for major ions in ^{3}He-rich flares, along with several representative UH ions. The figure shows the unique location of ^{3}He, and a yellow band at the ^{4}He gyrofrequency. The lines labeled 100K-10MK show average *Q/M* for the species at each temperature. As expected, the cyclotron frequencies for C-Fe move towards the yellow band (i.e. fully stripped) with increasing temperatures, eventually placing them in the region of the waves damped by the abundant ^{4}He. So with increasing temperatures, the *Q/M* ratio of heated species moves to the yellow band where heating is depleted compared with heavier species whose *Q/M* ratios fall below the frequency damped by ^{4}He. This can lead to an increase in the Fe/O ratio, but the reason is not due to the enhancement of Fe but rather the depletion of O. This is qualitatively consistent with the observed increase in Fe/O seen with increasing Fe ionization states (e.g., Klecker et al. 2007).

Figure 8 shows *Q/M* values for those neutron-rich nuclei of Ne, Mg, and Si which have abundances of at least a few percent of the main isotope. These neutron-rich nuclei have *Q/M* values that lie outside $Q/M = 0.5$, and thereby avoid depletion, as do Fe and the UH nuclei. Figure 9 explores this further with a plot of the fraction of major elements in the range C-Fe that have a *Q/M* ratio <0.49 as a function of temperature. The broad range of temperatures over which an element's fraction decreases is due to the distribution of multiple ionization states at each temperature: only fully ionized *Q/M* = 0.5 elements contribute to the decrease. At higher temperatures in the plot, the flattening of the C, Ne, Mg, and Si curves is due to their neutron-rich isotopes (assuming solar-system abundances, Lodders 2003, table 6). The plot assumes a limit of 0.49 for the damped wave region instead of the limit 0.44 in Roth & Temerin (1997) because the observed enhancements of neutron rich ^{25}Mg and ^{26}Mg would not occur with the 0.44 limit since they would fall into the damped wave range. Qualitatively Figure 9 shows that as temperatures increase above a few MK, O is depleted causing observed high Ne/O through Fe/O ratios. Above ~10 MK increasing fractions of Ne and Mg have *Q/M* ratios entering the damped wave region, which will result in high Si/O and S/O ratios.

The question arises about the strength of the damping: if it was extreme, then in principle the Fe/O ratio might reach extremely high values, but observations show it is almost always less than 2, limiting the size of the damping factor for heavy ions to less than a factor of ~10. In order to calculate an abundance pattern due to these effects, a reference population needs to be selected. Most candidates (e.g, slow solar wind, fast solar wind, coronal, low- and high-energy SEPs) are similar and we used the large SEP abundances from Desai et al. (2006) since they apply to an energy range close to the SIS observations. The main difference between this reference abundance and some others is that Fe/O ~0.4, instead of ~0.1. This affects the size of the damping factor by a factor of 2-3, and is not critical in the discussion below.

3.2 Comparison with the 2022 Nov. and 2023 Apr. ^{3}He-rich SEP events

The orange curves in both panels of Figure 6 show the abundance of heated ions, calculated starting with the reference population along with a damped wave region of $Q/M < 0.28$ or $Q/M > 0.49$. Minor isotope values were from Lodders (2003), and ionization states obtained from Mazzotta et al. (1998) who tabulated abundances of each individual ionization state for H-Ni over the temperature range 10^4 – 10^9 K. This leaves unspecified a factor for damped waves, which was treated as a free parameter of value ~0.1-1.0 times the undamped wave factor. Then for each temperature an abundance pattern for the elements was calculated by summing over the isotopes. For a damping factor of 1.0 (no damping) this procedure returns the reference population abundances at all temperatures. As the damping factor is decreased, for different temperatures isotopes falling into the damped region are weighted by the damping factor. For example, if the damping factor is 0.2, then at a temperature where 70% of the O falls in the damped region (about 3.5MK, see Figure 9), the relative abundance of O would be (0.3 + 0.7*0.2) or 0.44 of the reference. For this case the Fe/O ratio would then be ~2.3 times enhanced over the reference.

The orange line in the left panel of Figure 6 shows calculated abundances for 3.2 MK and a damping factor of 0.4. The right panel orange line fit uses a higher temperature, 10 MK, and stronger damping factor of 0.2. For O and heavier ions the calculated abundances are with some exceptions reasonably close to the observed pattern, in particular the enhancement of Si in the right versus left panel. The relatively high abundances of C and N in the right panel lie well above the calculation. **Another puzzling discrepancy is the low S value from the model seen in both panels of Fig. 6, but more pronounced for the 2023 April 8 event.** Since the H *Q/M* ratio lies outside the range considered in the model, agreement is not expected. However, ^{4}He is in the considered range, and perhaps serendipitously for the S-Si rich case in the right panel the value is not far from the model. This is not the case in the left "typical ^{3}He-rich" panel, whose low ^{4}He value in the 2022 November 9 event would imply damping factor ~10 times smaller than the one used. However for ^{4}He there are other considerations in the eventual energization such as differing Coulomb loss rates compared to heavy ions that might be important for ^{4}He but are beyond the scope of the calculation here (see discussion in Roth & Temerin 1997). Note that at the temperatures in Figure 6, the region of low damping with $Q/M < 0.28$ does not play a role for ions below Fe due to their high ionization states (see Figure 7).

3.3 Comparison with previous surveys of Fe ionization states and isotopic enhancements

Figure 10 explores other results from the model calculation, assuming a damping factor of 0.2 as in the Si-S rich event in Figure 6. The left panel shows the Fe/O ratio versus average ionization state of Fe plotted along with data from 18-event survey of Möbius et al. (2000, see their Table 1 and Figure 2). The survey included both large shock-associated SEP events and ^{3}He-rich events. Filled and open circles denote ^{3}He-rich and gradual SEP events, respectively, which were identified by re-examining the events in their table. The solid blue line shows the model calculation for temperatures above 3 MK, with a dashed blue line showing the reference population for lower temperatures which are presumably shock-associated events not addressed by the model.

Another feature of ^{3}He-rich events is the surprisingly large enhancement of neutron-rich isotopes such as ^{22}Ne/^{20}Ne, ^{26}Mg/^{24}Mg, etc. (Dwyer et al. 2001; Leske et al. 2001, 2007; Mason et al. 1994). The right panel of Figure 10 shows the calculated ^{22}Ne/^{20}Ne ratio versus Fe/Mg compared with observations below ~1 MeV nucleon^{-1} from Dwyer et al. (2001). As in the left panel, we re-examined the individual events and classified them as ^{3}He-rich (filled circles) or gradual (open circles). The model reasonably fits the enhanced values although the uncertainties are large. The enhancement compared to the reference population is roughly a factor of 4, about the same as the Fe/O enhancement in the same calculation. The rough equality of the ^{22}Ne/^{20}Ne enrichment and Fe/O enrichment has been a long-standing puzzle since the difference in *Q/M* ratio for the Ne isotopes is only 10%, while for Fe/O the difference is roughly 30% ([18/56]/[8/16]). Dwyer et al (2001) discussed this issue in detail. In the model presented here the similarity in enhancements for Fe/O and e.g., ^{22}Ne/^{20}Ne is expected since it is the depletion of the reference element (^{16}O, ^{20}Ne) that causes the effect and both are depleted by the effect of the damped waves.

Another long standing puzzle in ^{3}He-rich events is the lack of correlation between the ^{3}He/^{4}He ratio and the Fe/O ratio (e.g., Mason et al. 1986; Reames et al. 1994). Since the heavy ion enrichments are a fundamental property of ^{3}He-rich events, how could the degree of ^{3}He enrichment be uncorrelated with the Fe/O enrichment? In the mechanism explored here the solution lies in the mechanism wherein the Fe enrichment and ^{3}He enrichment are coming from different processes. First, the Fe/O enrichment comes from O depletion due to damping of waves corresponding to fully stripped $Q/M = 0.5$ ions. The ^{3}He is not heated by these damped waves but rather by those closer to its gyrofrequency. Viewed this way there is no reason to expect such a correlation, and its absence does not present a problem.

Although UH/O ratio will be enhanced by the mechanism discussed here, it will be no larger than the Fe/O enhancement since all Fe and UH fall below the damped wave cutoff (Figure 7) and so would participate equally. However, at the temperatures considered here most or all the *Q/M* values for UH nuclei are much lower than those for ^{4}He-Fe, so they might be in a different regime altogether. For example Eichler (1979, 2014) describes how the large gyroradii of UH nuclei could lead to preferential acceleration (see also Miller 1998, 2002; Miller & Reames 1996). These considerations are beyond the scope of this paper. However we note in the context of particle motion along a magnetic field gradient the large gyroradius of UH nuclei would lead to different mirroring altitudes which could play a role in the dynamics of the acceleration (e.g., Fitzmaurice et al. 2022).

In this model because the UH acceleration and O depletion are in essence decoupled, it is not physically meaningful to discuss a UH/O ratio in exploring UH enhancements. Rather the UH/Fe ratio appears more meaningful since the depletion of O is removed, and the challenge for particle acceleration is with respect to Fe. Figure 11 plots the UH enhancements compared to Fe from the 2022 November 9 event, and re-plots the UH enhancements from Mason et al. (2004) where they were originally shown compared to Oxygen. The fitted slope is the same as the earlier survey, however the enhancements required for the UH nuclei are smaller, ranging from ~6 (mass 78-100) to ~30 (mass 180-220). The pattern in the figure can be reasonably fitted if the acceleration factor in our model is a power law in *Q/M* with the slope shown, but such an addition is without physical motivation and not addressed in the model of Roth & Temerin (1997).

3.4 Conclusions

The calculation presented here explores implications of the preferential heating of species forming a seed population, and does not address other aspects such as spectral form, abundance ratios and ionization states increasing with energy, etc. We speculate that some of the energy dependences could be related to acceleration times wherein the additional time to accelerate particles to higher energies may also lead to further heating of the plasma and increased ionization states. Other types of accelerating plasma waves might serve as well as those in Roth & Temerin's model. Additionally, other mechanisms such as ion stripping may sometimes play a role (Kartavykh et al. 2020, 2008; Mason & Klecker 2018), but these mechanisms do not address the ^{3}He enrichment, nor can they reproduce the large enrichments of neutron rich isotopes of Ne and Mg. With these limitations in mind we suggest that the observations discussed here can provide a framework for a single mechanism operating in ^{3}He-rich events, namely (1) stochastic acceleration over a broad range of frequencies including ^{3}He, heavy ions through Fe, (2) a range of damped waves near the gyrofrequencies of abundant H and ^{4}He, (3) enhancement of heavy ions depending on temperature due to the depletion of fully stripped $Q/M = 0.5$ species which fall into the wave range damped by ^{4}He, (4) acceleration taking place in coronal loops which provide the required magnetic field gradient and the presence of emerging magnetic flux leading to reconnection, (5) access to interplanetary space through coronal holes or scattered open field lines, and (6) possible additional enhancement of UH nuclei compared to Fe due to wave cascading or some other mechanism involving their large gyroradii.

Acknowledgements

Solar Orbiter is a mission of international cooperation between ESA and NASA, operated by ESA. The Suprathermal Ion Spectrograph (SIS) is a European facility instrument funded by ESA under contract number SOL.ASTR.CON.00004. We thank ESA and NASA for their support of the Solar Orbiter and other missions whose data were used in this letter. Solar Orbiter post-launch work at JHU/APL is supported by NASA contract NNN06AA01C and at CAU by German Space Agency (DLR) grant # 50OT2002. The UAH team acknowledges the financial support by the Spanish Ministerio de Ciencia, Innovacion y Universidades MCIU/AEI Project PID2019-104863RBI00/AEI/10.13039/501100011033. I.R. acknowledges the support by NASA contract NNN06AA01C. N.V.N. acknowledges support by NASA grants 80NSSC18K1126 and 80NSSC20K028; R.B. acknowledges support by NASA grants 80NSSC21K1316 and 80NSSC22K0757; AR locations were from the daily reports prepared by the U.S. Dept. of Commerce, NOAA, Space Weather Prediction Center.

ORCID iDs

G. M. Mason https://orcid.org/0000-0003-2169-9618

I. Roth https://orcid.org/0000-0001-7661-5587

N. V. Nitta http://orcid.org/0000-0001-6119-0221

R. Bučík http://orcid.org/0000-0001-7381-6949

D. Lario http://orcid.org/0000-0002-3176-8704

G. C. Ho https://orcid.org/0000-0003-1093-2066

R. C. Allen https://orcid.org/0000-0003-2079-5683

A. Kouloumvakos https://orcid.org/0000-0001-6589-4509

R. F. Wimmer-Schweingruber https://orcid.org/0000-0002-7388-173X

J. Rodriguez-Pacheco http://orcid.org/0000-0002-4240-1115

TABLE 1

SOLAR PARTICLE EVENT AND SOLAR PROPERTIES

Event number	1	2
Event start day	2022 Nov 9	2023 Apr 8
Interval (Day of year)	313.25 – 313.90 [a]	98.75 – 99.25
Ion injection time (UT)	6:28 ± 0:15 [b]	20:58 ± 0:08 [b]
^{3}He Fluence [c] (particles/(cm^2 sr MeV/nuc))	7,200 ± 600	89,400 ± 2100
Fe Fluence [c] (particles/(cm^2 sr MeV/nuc))	19,200 ± 950	1,720 ± 340 [d]
^{3}He/^{4}He [c]	**1.35 ± 0.27**	5.5 ± 0.3
Fe/O [c]	2.66 ± 0.25	2.0 ± 0.7 [d]
Si/O [c]	**0.40 ± 0.06**	**2.69 ± 0.64 [d]**
Si/S [c]	**1.32 ± 0.24**	**1.30 ± 0.30 [d]**
(mass > 100 amu)/Fe × 10^3 (100-900 keV nucleon^{-1})	3.2 ± 0.7	< 2.7 [e]
Solar Orbiter radial distance (au)	0.59	0.29
Solar Orbiter separation angle with Earth	23.7°	48.3°
Nearby Active Regions	13140, 13141	13270
Active Region location on day of event	N26E03, N14E13	S24W73
Magnetically connected Solar Orbiter?	Y if slow SW	Y
Electron event injection	6:00 [f]	…
Jets	weak or none	weak or none
Type III burst	Y (<1 MHz)	Y (weak)

Notes.

[a] time intervals adjusted for velocity dispersion as described by Mason et al. (2000)

[b] injection time uncertainty based on ~10% field line meandering uncertainty and 350 keV nucleon^{-1} ion flight time

[c] energy interval: 320-452 keV nucleon^{-1}

[d] ratio not available at higher energy; result is value from 226-320 keV nucleon^{-1}

[e] 1 count upper limit

[f] dispersionless onset

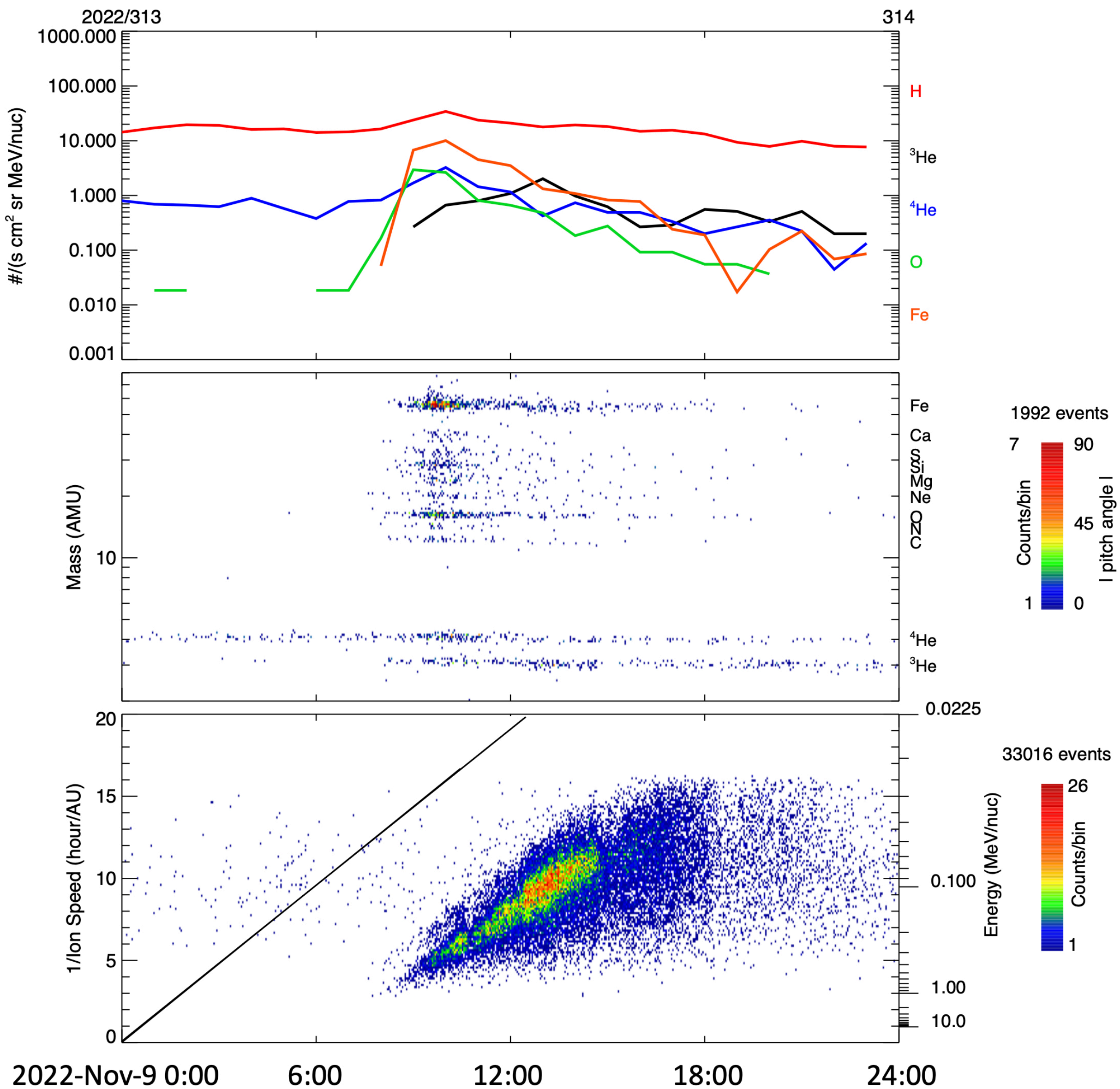

Figure 1. ^{3}He-rich SEP event starting 2022 November 9. *Top panel:* Time profiles of H, ^{3}He, ^{4}He, O and Fe ions of 0.23 – 0.32 MeV nucleon^{-1}. *Middle panel:* Mass spectrogram for elements from He to Fe for ions with energies 0.3-10 MeV nucleon^{-1}. *Bottom panel:* Plot of 1/ion speed vs. time of arrival for ions of mass 10-70 AMU. The oblique line indicates the arrival times assuming an Archimedes spiral magnetic path length of 0.61 au.

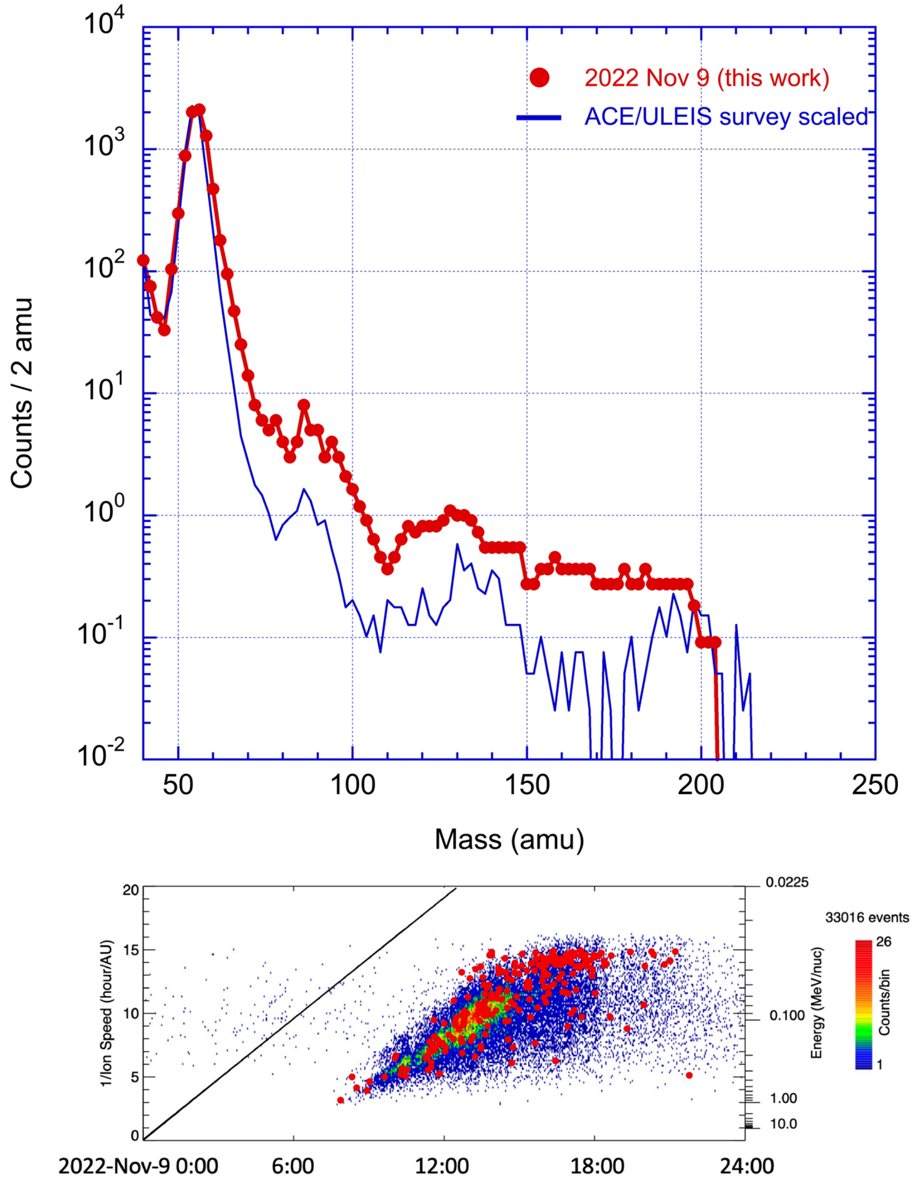

Figure 2. *Upper panel:* Red filled circles: mass histogram of ions with energies above 100 keV nucleon^{-1} for 2022 November 9 event. Blue line: histogram of ions 0.15-0.5 MeV nucleon^{-1} from survey by Mason et al. (2004), normalized to 2022 event Fe peak. *Lower panel:* 1/ion speed vs. time of arrival from Figure 1 with filled red circles showing arrival times of **individual** ions with mass > 80 amu.

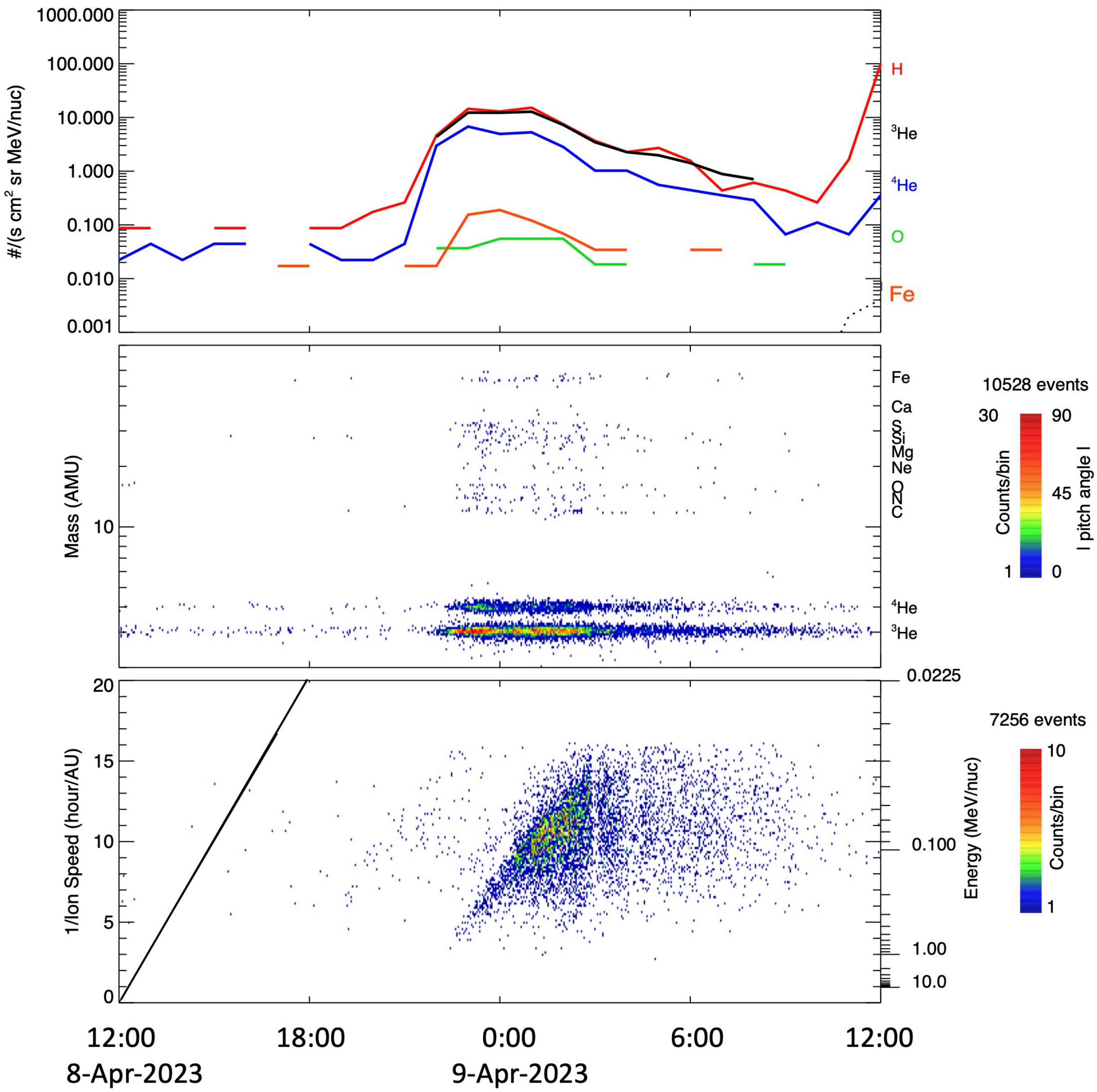

Figure 3. Same as Figure 1 for ^{3}He-rich SEP event starting 2023 April 8, except middle panel energy range is 0.2-10 MeV nucleon^{-1}, and bottom panel oblique line is for a path length of 0.29 au.

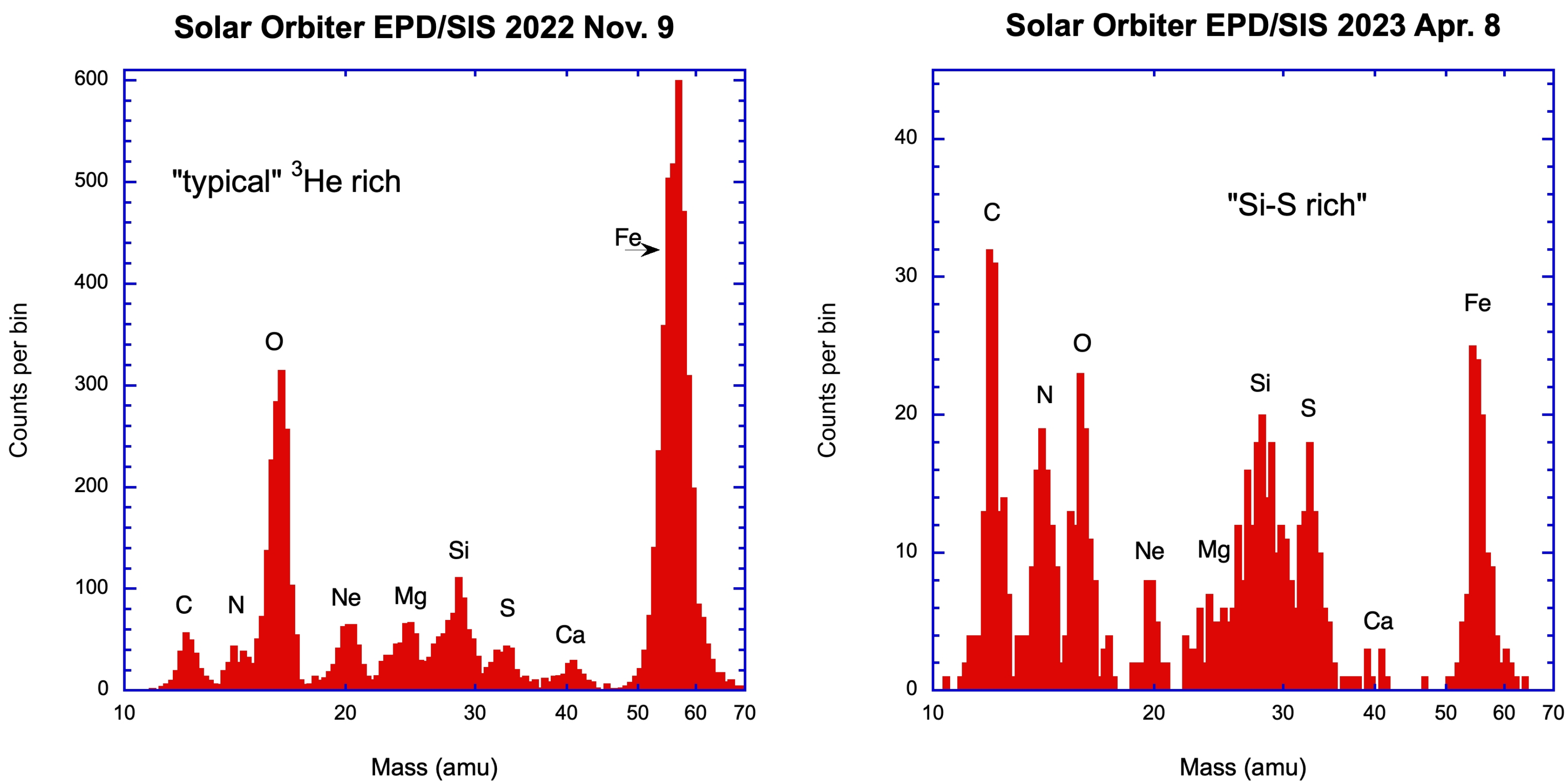

Figure 4. Mass histograms for C through Fe ions with energies above 150 keV nucleon^{-1}. Left panel: 2022 November 9 event showing mass enhancement of heavy ions typical of ^{3}He-rich events. Right panel: 2023 April 8 mass histogram showing enhancement pattern of relatively rare ^{3}He-rich events rich in Si and S

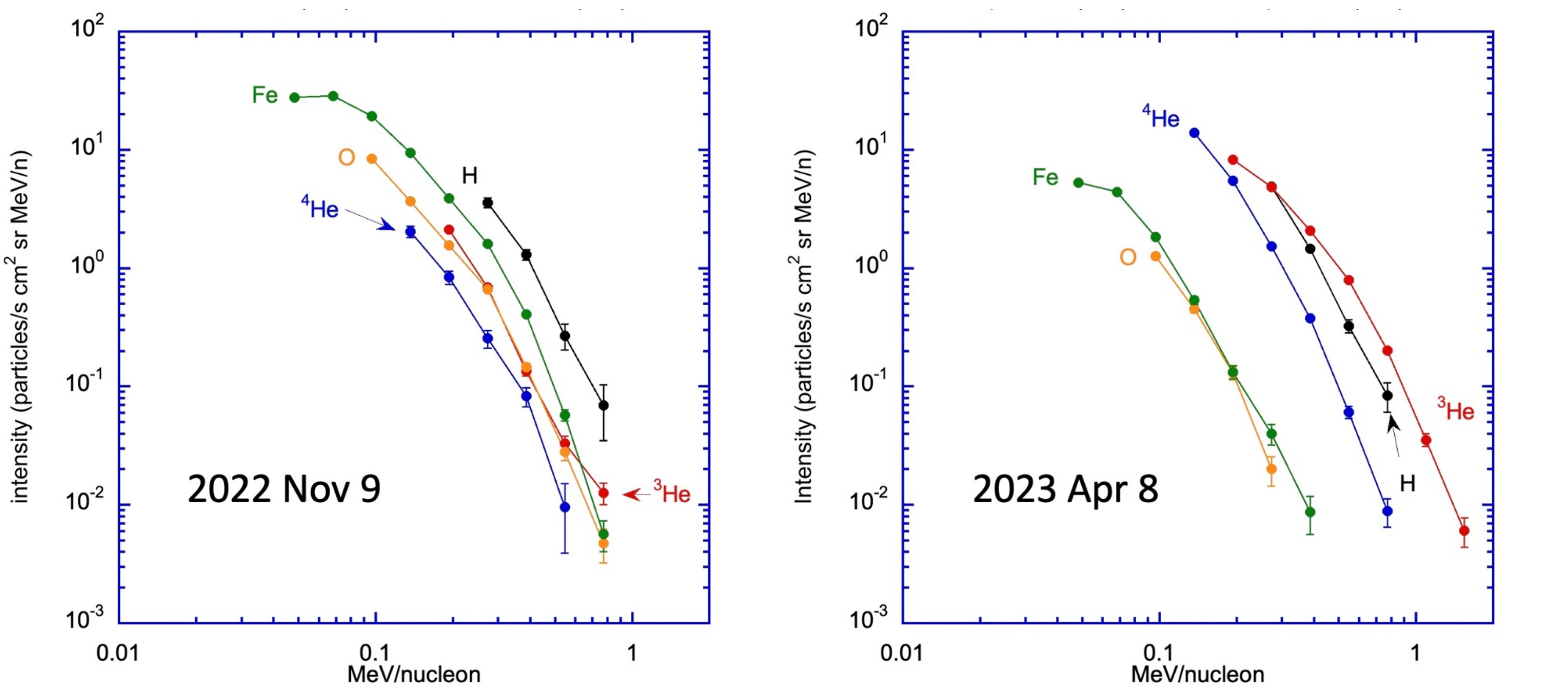

Figure 5. Event averaged differential energy spectra for the two events. Left panel: 2022 November 9 event showing unusually high Fe exceeding ^{4}He. Right panel: 2023 April 8 event with ^{3}He exceeding protons above ~400 keV nucleon^{-1}. Both events show H:^{4}He ratios much lower than typical solar energetic particle populations.

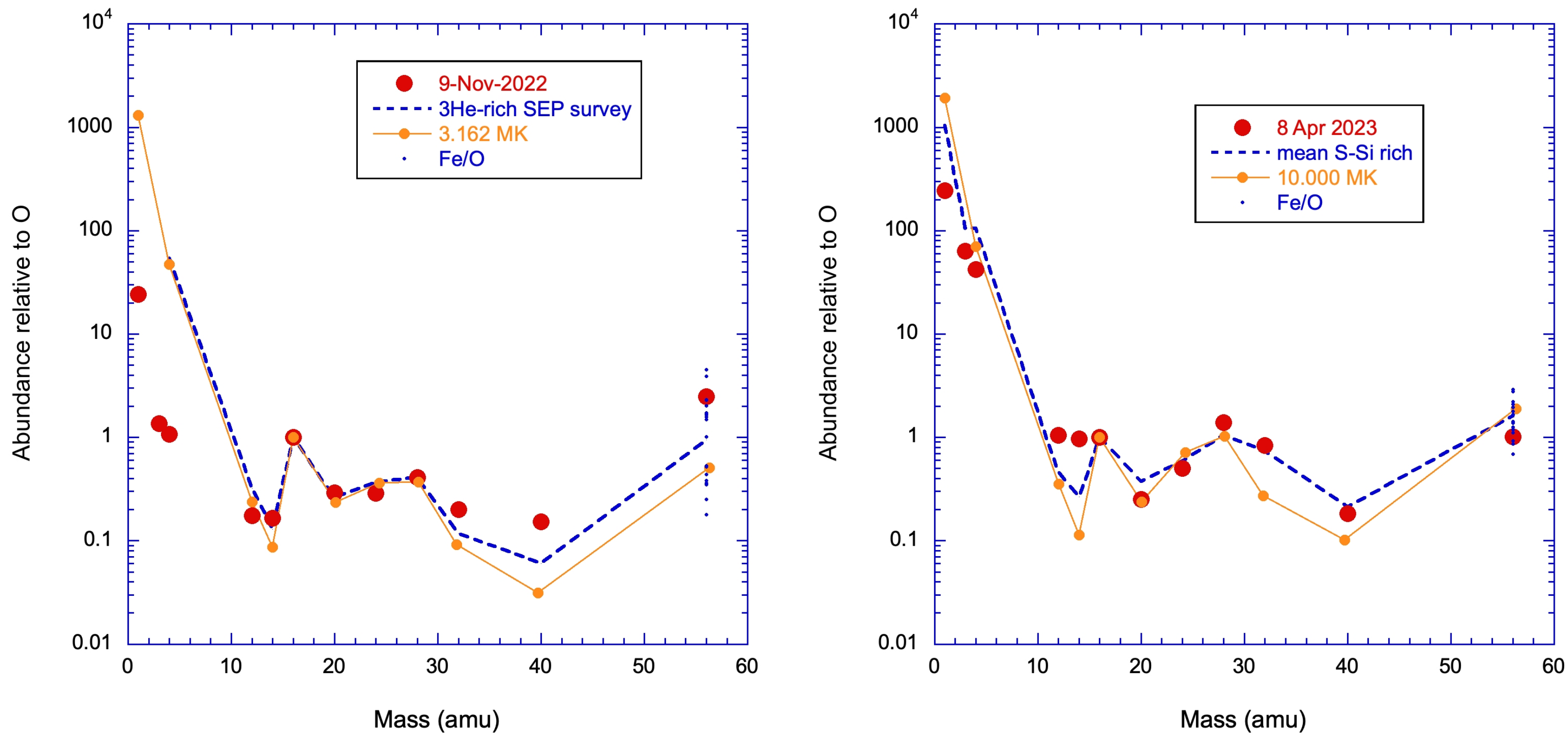

Figure 6. Filled red circles: heavy ion abundances relative to O from160-226 keV nucleon^{-1} for both events (proton abundances from 226-320 keV nucleon^{-1}); dashed blue lines: abundances from (left) a ^{3}He-rich event survey (Mason et al. 2004) and (right) a survey of Si-S rich ^{3}He-rich events (Mason et al. 2016); Orange lines: model calculations of abundances at (left) 3.2 MK and (right) 10 MK (see text for details). All abundances normalized to O = 1.

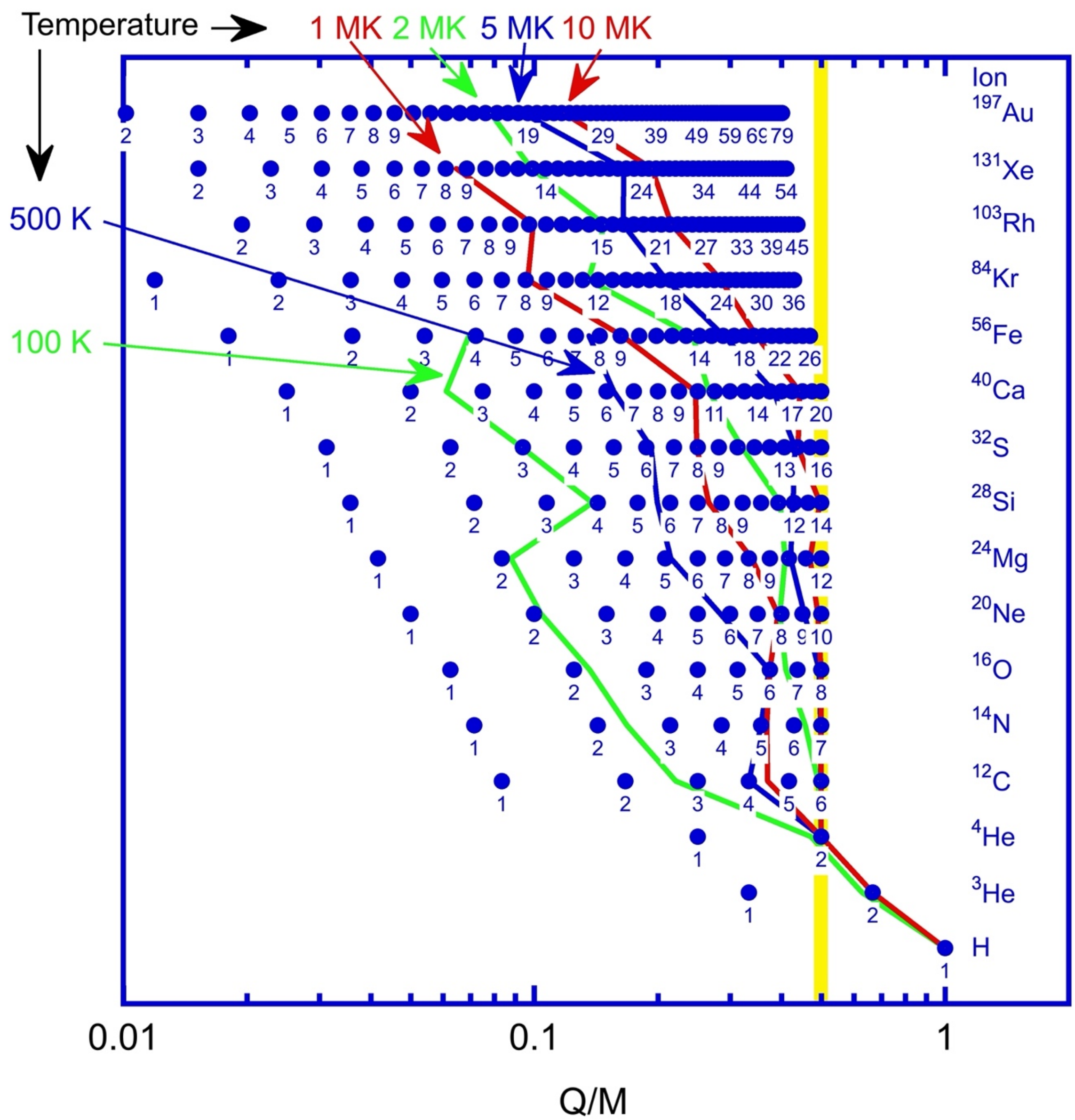

Figure 7. *Q/M* ratios (atomic charge/amu) for different major ion species with ionization state shown by the number below each point. The y-axis is arbitrary to separate the species. Lines at 100K, 500K, etc. show average ionization state for an equilibrium plasma (Mazzotta et al. 1998; Post et al. 1977). The thick yellow line shows *Q/M* where acceleration is suppressed due to damping of plasma waves by ^{4}He.

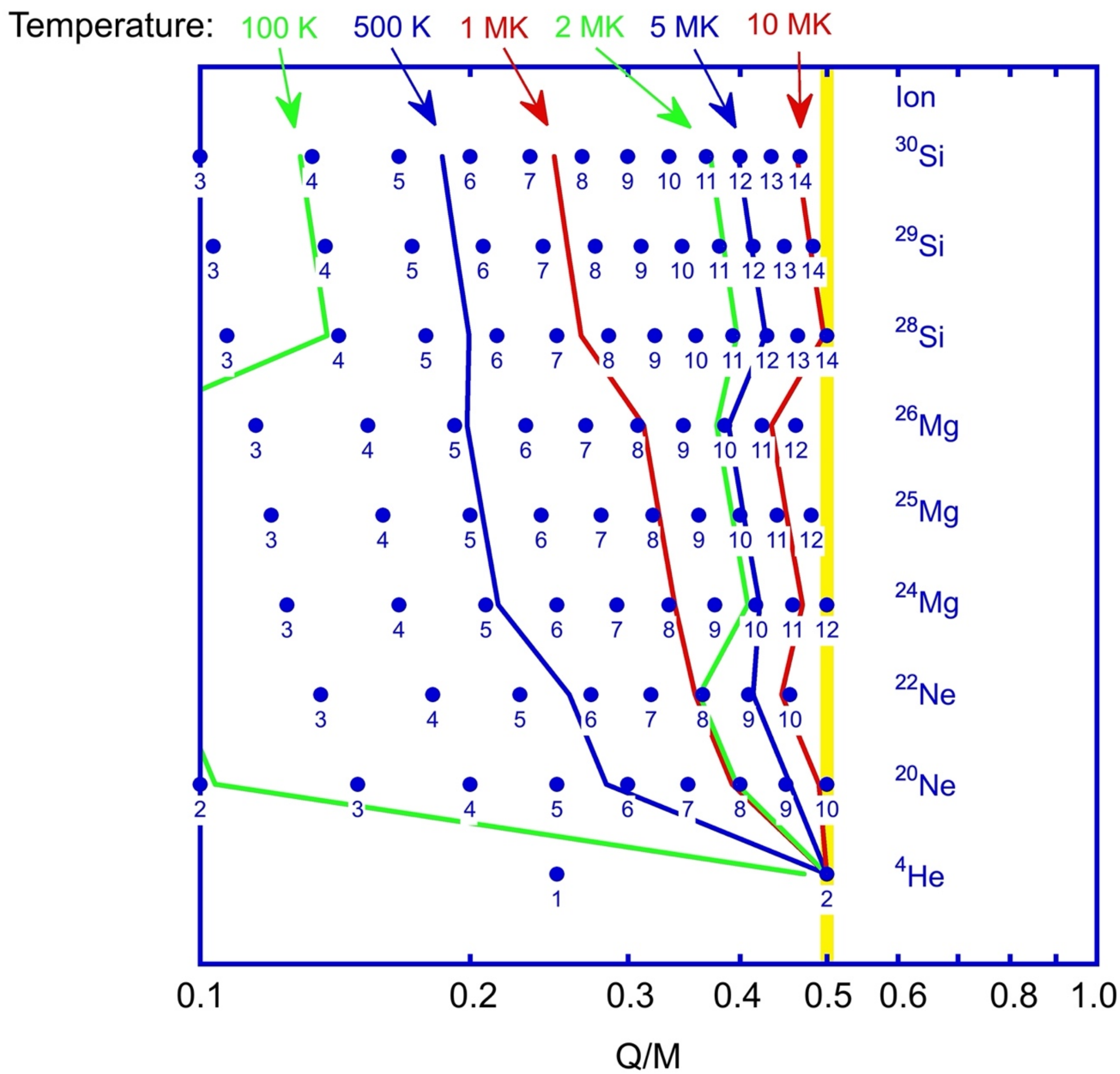

Figure 8. Same as Figure 7 showing neutron-rich isotopes of Ne, Mg, Si, which lie below *Q/M* = 0.5, which is damped by ^{4}He.

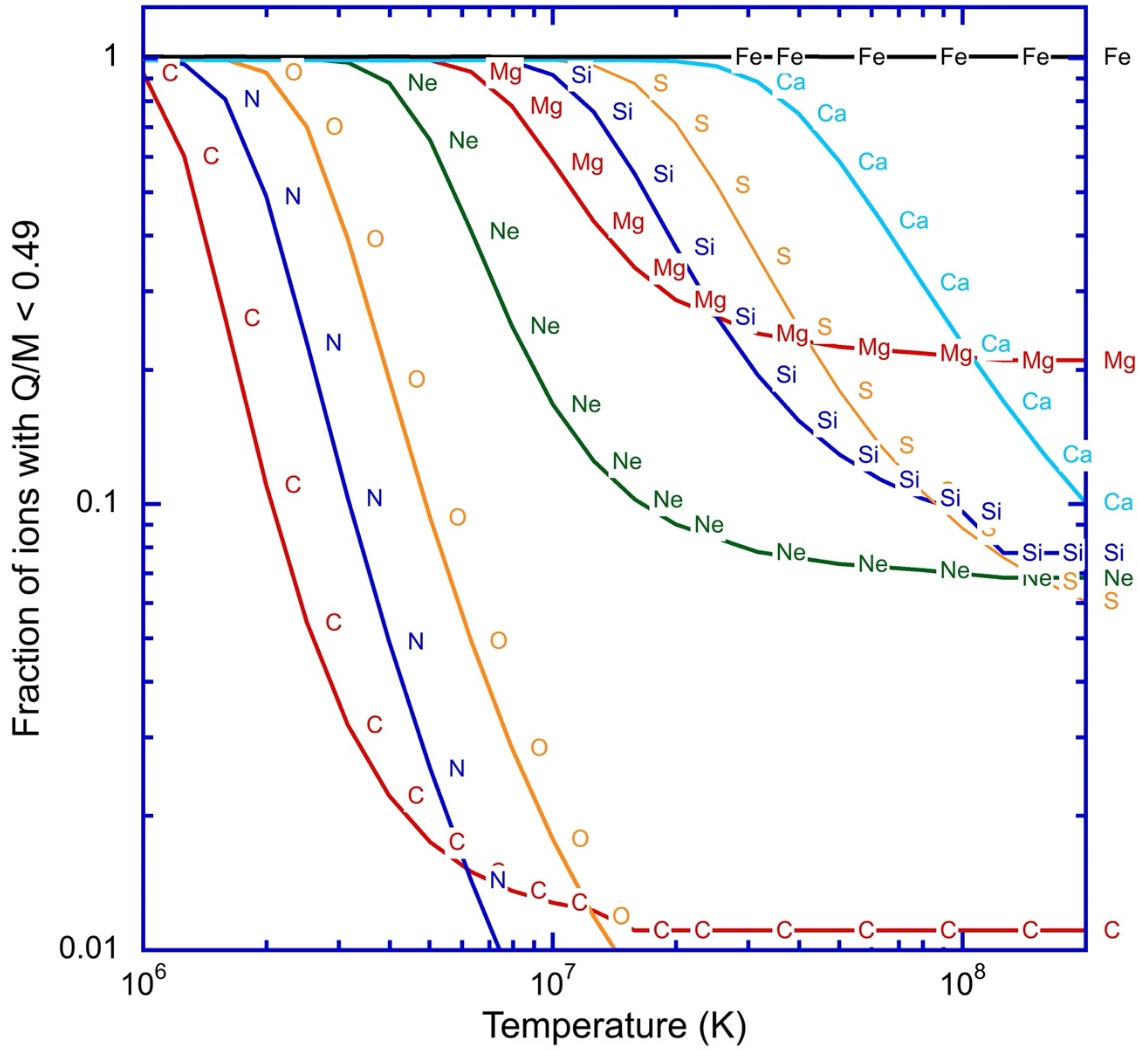

Figure 9. Fraction of each element whose *Q/M* ratio falls below the damped wave region in Figures 7 and 8 versus temperature. Flattening of some curves at high temperatures is due to neutron-rich minor isotopes: ^{13}C, ^{22}Ne, ^{25}Mg, ^{26}Mg, etc.

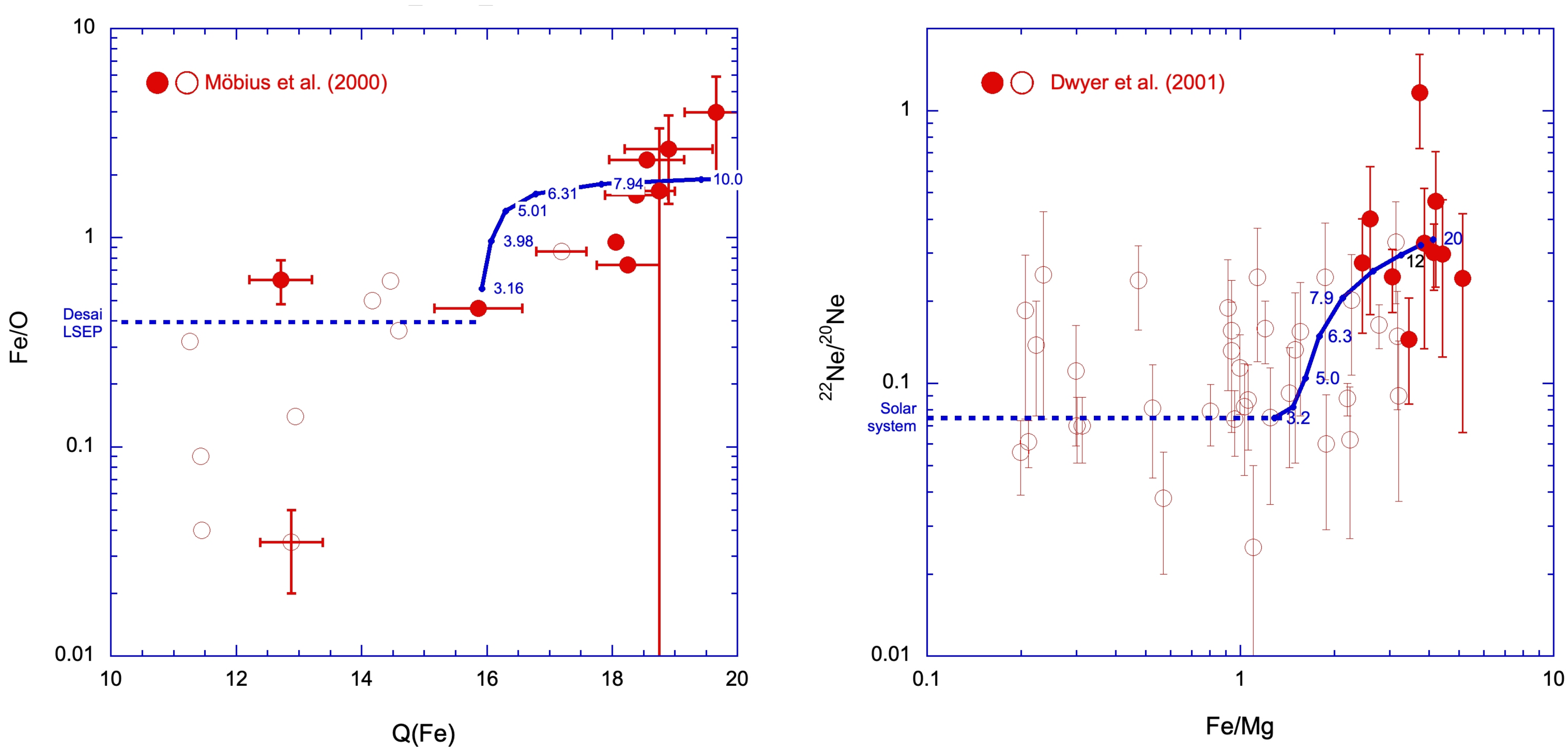

Figure 10. Left panel: Fe/O versus Fe ionization state; Right panel: ^{22}Ne/^{20}Ne vs Fe/Mg ratio. Circles are observations from the surveys of Möbius et al. (2000) and Dwyer et al. (2001). Filled circles are impulsive SEP events, open circles are gradual SEP events. Solid blue line shows model calculation with annotations showing temperature in MK. Dashed blue line is ratio from reference population.

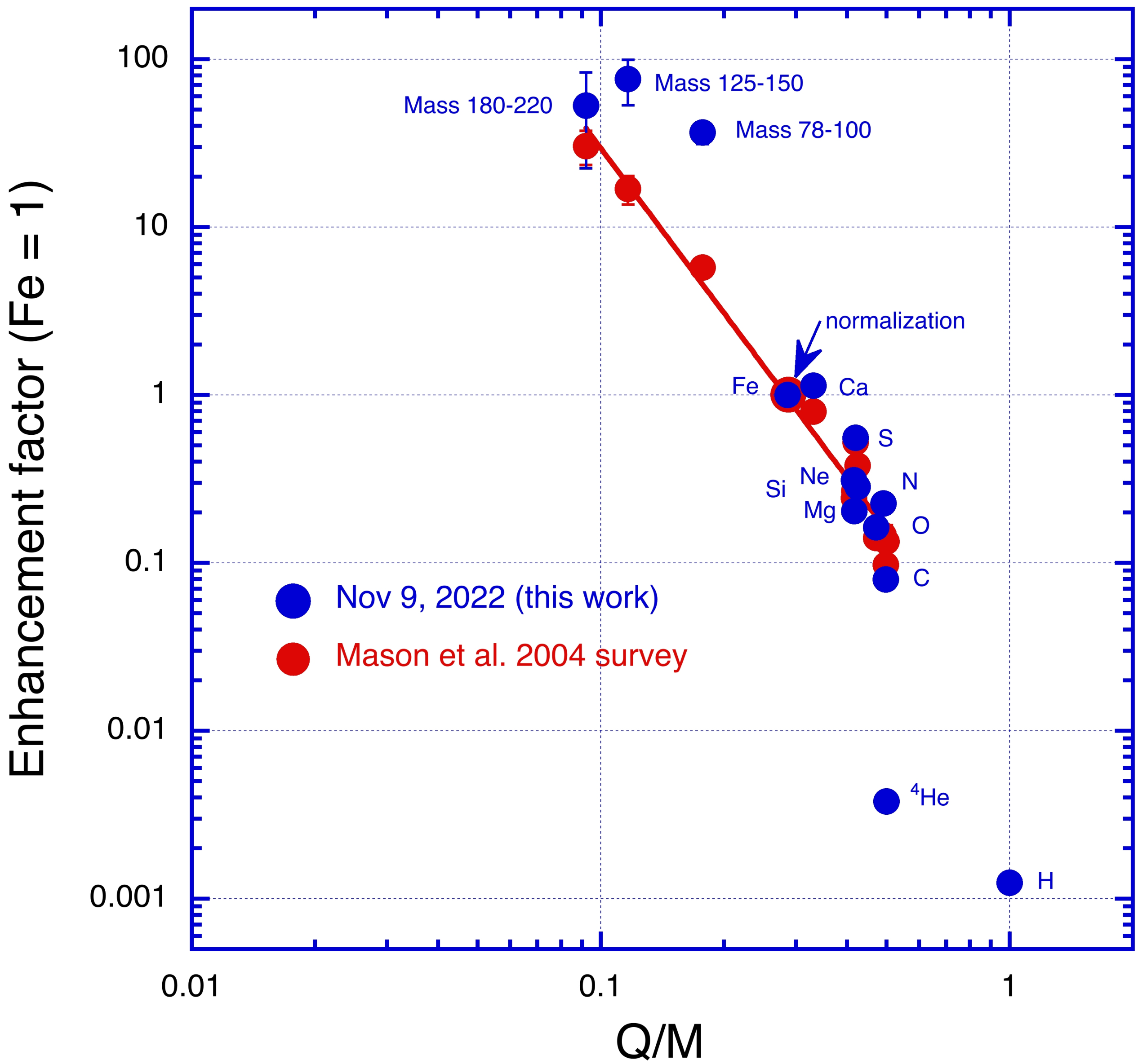

Figure 11. Enhancement of ions vs *Q/M* compared to gradual SEP events and solar-system abundances (above Fe). Red points from Mason et al. (2004) survey; blue points from 2022 November 9 event. Fitted slope of power-law fit to red points is -3.26.

References

Anders, E., & Grevesse, N. 1989, Geochim Cosmochim Acta, 53, 197
Bučík, R., Mason, G. M., Nitta, N. V., et al. 2023, Astron Astrophys, 673, L5
Desai, M., & Giacalone, J. 2016, Living Rev Sol Phys, 13, 3
Desai, M. I., Mason, G. M., Gold, R. E., et al. 2006, Astrophys J, 649, 470
Dwyer, J., Mason, G. M., Mazur, J. E., et al. 2001, Astrophys J, 563, 403
Eichler, D. 1979, Astrophys J, 229, 413
Eichler, D. 2014, Astrophys J Suppl Ser, 794, 6
Fitzmaurice, A., Drake, J. F., & Swisdak, M. 2022, in AGU Fall Meeting Abstracts, Vol. 2022, SH52E
Ho, G. C., Mason, G. M., Allen, R. C., et al. 2022, Front Astron Space Phys, 9, https://doi.org/10.3389/fspas.2022.939799
Kartavykh, Y. Y., Dröge, W., Klecker, B., et al. 2008, Astrophys J Suppl Ser, 681, 1653
Kartavykh, Y. Y., Dröge, W., Klecker, B., Kovaltsov, G. A., & Ostryakov, V. M. 2020, Astrophys J, 888, 48
Klecker, B., Mobius, E., & Popecki, M. A. 2007, Space Sci Rev, 130, 273
Kollhoff, A., Kouloumvakos, A., Lario, D., Dresing, N., & Gomez-Herrero, R. 2021, Astron Astrophys, 656, A20
Krucker, S., Hurford, G. J., Grimm, O., & et al. 2020, Astron Astrophys, 642
Lemen, J. R., Title, A. M., Akin, D. J., et al. 2012, Sol Phys, 275, 17
Leske, R. A., Mewaldt, R. A., Cohen, C. M. S., et al. 2007, Space Sci Rev, 130, 195
Leske, R., Mewaldt, R. A., Cohen, C. M. S., et al. 2001, AIP Conf Proc, 598, 127
Lodders, K. 2003, Astrophys J Suppl Ser, 591, 1220
Maksimovic, M., Bale, S. D., Chust, T., & Khotyaintsev, Y. 2020, Astron Astrophys, 642, A12
Mason, G. M., Fisk, L. A., Gloeckler, G., & Hovestadt, D. 1980, Astrophys J, 239, 1070
Mason, G. M., & Klecker, B. 2018, Astrophys J, 862, 7
Mason, G. M., Mazur, J. E., & Dwyer, J. R. 2002, Astrophys J, 565, L51
Mason, G. M., Mazur, J. E., Dwyer, J. R., et al. 2004, Astrophys J, 606, 555
Mason, G. M., Mazur, J. E., & Hamilton, D. C. 1994, Astrophys J, 425, 843
Mason, G. M., Nitta, N. V., Wiedenbeck, M. E., & Innes, D. E. 2016, Astrophys J, 823, 138
Mason, G. M., Reames, D. V., Von Rosenvinge, T. T., Klecker, B., & Hovestadt, D. 1986, Astrophys J, 303, 849
Mazzotta, P., Mazzitelli, G., Colafrancesco, S., & Vittorio, N. 1998, Astron Astrophys Suppl, 133, 403
Miller, J. A. 1998, Space Sci Rev, 86, 79
Miller, J. A. 2002, Multi-Wavel Obs Coronal Struct Dyn – Yohkoh 10th Anniv Meet Proc Conf Held Sept 17-20, 387
Miller, J. A., & Reames, D. V. 1996, AIP Conf Proc, 374, 450
Möbius, E., Klecker, B., Popecki, M. A., et al. 2000, ed. R. A. Mewaldt, J. R. Jokipii, M. A. Lee, E. Möbius, & T. H. Zurbuchen, Vol. 528 (AIP Conf Proc), 131
Müller, D., Cyr, O. C. S., Zouganelis, I., Gilbert, H. E., & Marsden, R. 2020, Astron Astrophys, 642, A1
Petrosian, V. 2008, arXiv.org, 1757

Petrosian, V. 2012, Space Sci Rev, 173, 535
Post, D. E., Jensen, R. V., Tarter, C. B., Grasberger, W. H., & Lokke, W. A. 1977, At Data Nucl Data Tables, 20, http://adsabs.harvard.edu/abs/1977ssrc.rept.....P
Reames, D. V. 2000, Astrophys J Suppl Ser, 540, L111
Reames, D. V. 2018, Space Sci Rev, 214, 61
Reames, D. V. 2021, Front Astron Space Sci, 8, 164
Reames, D. V., Meyer, J. P., & Von Rosenvinge, T. T. 1994, Astrophys J Suppl Ser, 90, 649
Rochus, P., Auchere, F., & Harra, L. 2020, Astron Astrophys, 642
Rodríguez-Pacheco, J., Wimmer-Schweingruber, R. F., Mason, G. M., et al. 2020, Astron Astrophys, 642, A7
Roth, I., & Temerin, M. 1997, Astrophys J, 477, 940
Rouillard, A. P., Pinto, R. F., Vourlidas, A., et al. 2020, Astron Astrophys, 642, A2
Temerin, M., & Roth, I. 1992, Astrophys J, 391, L105
Wang, L., Lin, R. P., Krucker, S., & Mason, G. M. 2012, Astrophys J Suppl Ser, 759, 69
Wiedenbeck, M. E., Mason, G. M., Cohen, C. M. S., et al. 2005, in ICRC 29 (Tata Inst. Fund. Res.), 117
Wimmer-Schweingruber, R. F., Janitzek, N. P., Pacheco, D., et al. 2021, Astron Astrophys, 656, A22